Elastic Stability of Shallow Bending-Active Arches

Elastic Stability of Shallow Bending-active Arches

Gianfranco Piana[1][0000-0002-3462-0203], Fabio Bazzucchi[2][0000-0002-2624-6944] and Amedeo Manuello[1][0000-0003-1474-0176]

[1] Department of Structural, Geotechnical and Building Engineering, Politecnico di Torino, Italy
[2] Senseable City Lab, Massachusetts Institute of Technology, Cambridge, MA
gianfranco.piana@polito.it

Abstract. We present a numerical and experimental investigation on the nonlinear equilibrium paths and elastic stability of pinned shallow arches realized by buckling a straight strut and then subjected to a transverse central point load. Finite element analyses were run to compare the behavior of arches with and without initial pre-stress condition. The effects of initial shallowness ratio, axial-to-bending stiffness ratio, and initial geometric imperfections on the equilibrium path and bifurcation points were investigated. As an experimental verification, laboratory tests were conducted on a pinned-pinned shallow arch obtained by buckling a thin, slender steel bar. Static and dynamic measurements were carried out to determine the load-displacement curve, the subsequent static deformed configurations, the frequency-load curves, and the buckling load. The acquired data were used for buckling load predictions and to obtain stability domains in terms of form factors and imperfection-sensitivity parameters.

Keywords: Snap-through Buckling, Elastic Stability, Nonlinear Bifurcation, Shallow Arch, Experimental Test, Finite Element Analysis.

1 Introduction

The behavior of pre-stressed arches intrigued for a long time the research in the field structural mechanics. Since the first experimental campaign by Roorda in 1965 [1,2], the effect of pre-stressing on the buckling of arches put into shape by overcritical compression of a straight strut has proven difficult to determine in a direct way. The difficulties to overcome are many and of many species. From a theoretical standpoint (both in analytical and numerical frameworks), the geometrically nonlinear nature of the problem requires computational efforts in taking into account initial pre-stressing and imperfections while deriving the equilibrium path in different loading and geometrical conditions. Experimentally, imperfection sensitivity together with uncertainties regarding structure's stiffness, strength, geometry, actual constraint conditions, and loading transmission, pose another layer of complexity.

Simple closed-form solutions were found for the *linear* buckling load of pre-stressed arches, allowing to compare the load bearing capacity to that of the corresponding non pre-stressed arch [3]. However, investigating the *nonlinear* equilibrium

path and buckling load requires approximate (analytical or numerical) solutions; furthermore, the above-mentioned difficulties and uncertainties make a direct comparison between experimental and numerical results very difficult; e.g. see [4].

As is well known, deep arches tend to loose stability by classic (linear) Euler buckling, whereas flat arches tend to loose stability by (non-linear) snap-through buckling. The former phenomenon is principally driven by the bending stiffness, while the latter is mainly governed by the axial stiffness. In the intermediate shallowness range, both axial and bending stiffness play a crucial role, so branching bifurcation of the nonlinear equilibrium path becomes possible, with a consequent reduction in loading capacity; initial (geometric or loading) imperfections further reduce the carrying capacity and favor the occurrence of the nonlinear limit-point (i.e. fold) bifurcation at lower loading levels. The phenomenon is governed by the shallowness ratio and by the axial-to-bending stiffness ratio of the arch. In this complicated scenario, the effect of a possible initial pre-stressing, introduced in the arch prior to the application of the additional transverse load, is not easy to determine.

In this contribution, we present part of the results of a work-in-progress about the matter. In particular, we show the results of an experimental campaign on the elastic stability of a slender, thin arch formed by a post-buckled straight beam and then subjected to a central point load. Load-displacement curves allowed to derive the equilibrium paths, thus reducing a continuous structure to a one-degree-of-freedom system. At the same time, a systematic geometry identification was carried out to determine the arch line configurations during the loading process and used to derive form factors for the buckling mechanism. High-frame rate cameras were also used to record the deflected shapes up to buckling. Moreover, the fundamental resonant frequency decay with the loading was measured, allowing for a buckling load prediction based on extrapolation [5]. Resting on this multi-level identification, we carried out a parametric ensemble of numerical analyses to provide stability domain predictions in terms of form factors and imperfection sensitivity. Results are in good accordance with experiments and enforce the importance of the problem, especially towards today's architectural trend of bending-active structures [6]. More results, with respect to what is shown here, will be presented at the Conference and in future contributions.

2 Problem Definition

Let us consider the plane problem of a pinned arch of span l_0 and rise f_0, obtained by buckling a slender straight beam of length l_n, under the action of an incremental central point load F (Fig. 1a). The arch (beam) is made of elastic material with Young's modulus E, shear modulus G, and is characterized by axial rigidity EA, bending rigidity EI, and shear rigidity GA_s, being A the area, I the principal bending moment of inertia, and A_s the shear-shape modified area of the cross-section ($A_s = A/t$, with t the shear factor). In particular, we consider a thin rectangular cross-section, of width b and thickness $h << b$. Thus: $A = bh$, $I = bh^3/12$, $A_s = 5/6\ A$; here, the effects of shearing deformability are small and can be neglected.

We call C_n the natural (i.e. stress-free) configuration, characterized by the strain state $\boldsymbol{\varepsilon_n} = \mathbf{0}$ and stress state $\boldsymbol{\sigma_n} = \mathbf{0}$. Applying an end shortening δ_0 to the straight beam, so that the beam results compressed by the post-critical force $P_0 > \pi^2 EI/l_n^2$, it reaches the pre-stressed configuration C_0, characterized by the strain state $\boldsymbol{\varepsilon_0}$ and stress state $\boldsymbol{\sigma_0}$ of the buckled beam (which is compressed and bent). Finally, applying an incremental central force F in the pre-stressed configuration C_0, the structure reaches the current (varied) configuration C, characterized by the strain state $\boldsymbol{\varepsilon}$ and stress state $\boldsymbol{\sigma}$. In Fig. 1b we have the corresponding arch where the initial curved shape coincides with the natural (stress-free) configuration, subject to the same incremental central point load F. In both cases, we call η the midpoint vertical displacement (different in the two cases) under the applied force F.

We are interested into investigating the elastic stability of the current configuration C, with respect to the applied force F, for the pre-stressed arch in Fig. 1a and for the corresponding non pre-stressed arch in Fig. 1b.

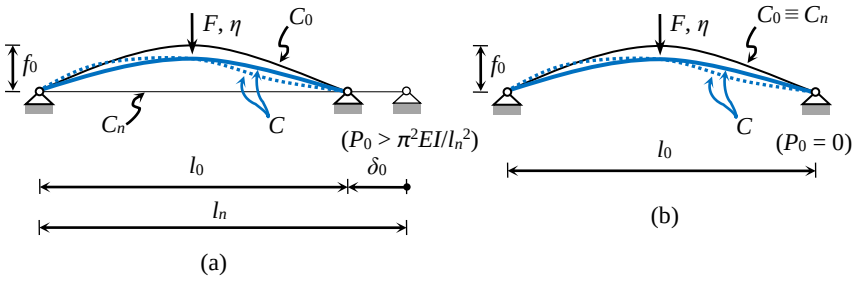

Fig. 1. (a) Pre-stressed arch made of a buckled strut, subject to incremental central point load and (b) corresponding non pre-stressed arch subject to incremental central point load. C_n is the natural (stress-free) configuration, C_0 is the pre-stressed configuration, and C is the current (varied) configuration.

3 Finite Element Analyses

Finite element analyses were run in LUSAS software (version 19.0-3 [7]). The arches were modelled by 20 nonlinear thick beam elements (BM131, a 3-node beam element with axial, bending and shearing deformability). Two different analysis typologies were conducted: linear eigenvalue (frequency and buckling) and nonlinear static. As for the eigenvalue analysis, full frontal solver was used, whereas for the nonlinear analysis a co-rotational formulation with arc-length was employed as the solution scheme. The nonlinear analyses used a prescribed displacement at the crown node to derive the equilibrium path, extracting the relevant vertical reaction (F). To initialize every analysis, a 1% of the total load factor was engaged. Nonlinear analyses were also used to apply the pre-stress by means of a prescribed support displacement. In such case, the equilibrium path with respect to the crown displacement was derived so to keep the internal stress / strain state introduced by the support displacement active.

The same was done also for the frequency linear eigenvalue analysis, repeated at several load steps (i.e. different prescribed crown vertical displacements).

Several analyses were conducted to compare the behavior of arches with and without initial pre-stress. The effects of initial shallowness ratio, axial-to-bending stiffness ratio, and initial geometric imperfections on the equilibrium path and bifurcation points were investigated. Here, only the simulations related to the structure having the same features of the arch tested in the lab will be discussed. The input parameters adopted in the simulations are the following: rectangular cross-section with width b = 20 mm and thickness h = 1.5 mm (A = 30 mm^2, I = 5.625 mm^4, A_s = 25 mm^2); isotropic, linearly elastic material with Young's modulus E = 196,968.18 MPa and Poisson's ratio v = 0.3 (see Subsection 4.1); straight beam length l_n = 1,114 mm, prescribed end displacement (end "shortening") δ_0 = 14 mm, producing the target values of arch span l_0 = 1,100 mm and arch rise f_0 = 77 mm. Hinged boundary condition was considered at the ends in all simulations.

The main results are summarized in the next subsection.

3.1 Numerical Results

Fig. 2 shows the load (F) vs. displacement (η) curves of pre-stressed and non pre-stressed arches. The force F is the vertical reaction (numerical output) corresponding to the imposed crown vertical displacement (numerical input). In Fig. 2 we see that the pre-stressing reduces the slope (stiffness) of the ascending (pre-critical) branch and strongly diminishes the buckling load (i.e. the peak in the equilibrium path). For both cases, stability is lost by nonlinear bifurcation, the asymmetric deformed shape being the critical one. In the same figure, three deformed shapes are shown for the case with no pre-stress (load steps 1, 7, 20) and one for the case with pre-stress (load step 20). Still in Fig. 2, the linear buckling load is also marked: note that this value is the same for the two cases since the Euler critical value of the force F, obtained *via* a buckling linear eigenvalue analysis, is not affected by the pre-stress (the geometric stiffness matrix only considers the effect of the force F).

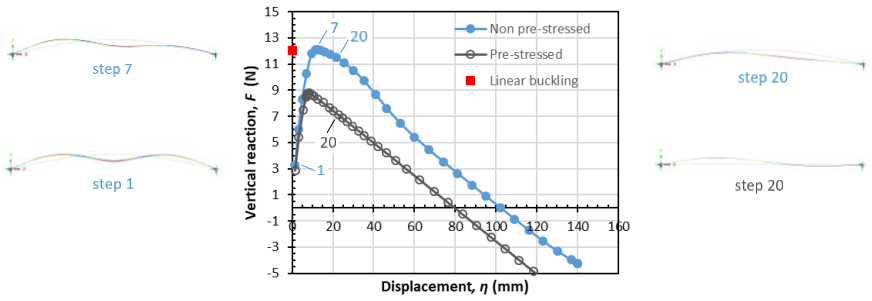

Fig. 2. Comparison between load vs. displacement (F – η) curves of pre-stressed and non pre-stressed arches.

Fig. 3a shows the fundamental frequency (f_1) vs. load (F) curves for the arches with and without pre-stress. Again, the stiffness reduction induced by the pre-stressing is evident. Fig. 3b shows the square of the fundamental frequency normalized to its initial value for $F = 0$ ($f_{1,0}$), vs. the force F for the two cases; note that these latter diagrams are linear. As is well known, the zero frequency condition can be used to predict the (static) buckling load [5,8]; see Subsection 4.3.

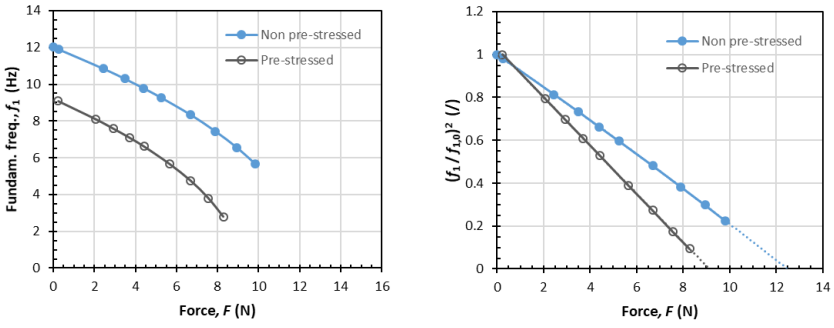

(a) (b)

Fig. 3. (a) Comparison between fundamental frequency vs. load ($f_1 - F$) curves of pre-stressed and non pre-stressed arches. Part (b) shows the normalized fundamental frequency squared vs. the force F.

4 Experimental Tests on a Pre-stressed Shallow Thin Arch

Laboratory tests were conducted on a pre-stressed, shallow thin steel arch. The arch had rise $f_0 = 77$ mm and span $l_0 = 1{,}100$ mm, obtained by axial buckling of a thin steel bar having length $l_n = 1{,}114$ mm. The arch was constrained in the vertical plane by cylindrical hinges at the ends (Fig. 4). The tested structure was characterized by the following non-dimensional parameters: slenderness ratio of the initially straight bar, $l_n / (I/A)^{0.5} = 2{,}573$; rise-to-span ratio, $f_0 / l_0 = 0.07$; slenderness ratio of the arch (buckled bar), $EAl_0^2 / EI = 6.45\text{E+}06$.

The tests were conducted by controlling (imposing) the vertical central force, realized in a quasi-static manner by filling a container with known quantities of fine sand, connected to the arch midpoint by a nylon line. Static displacement measurements were conducted by a Leica TCR1201 total station; the specimen was provided 11 targets along the arch line (Fig. 4b). The fundamental resonant frequency was extracted for increasing values of the applied force by analyzing the free response consequent to a small external impulsive excitation. The free dynamic response was measured at a point, located at about quarter-span, by a optoNCDT 1302-20 laser displacement transducer by Micro-Epsilon (Fig. 4a); this transducer has 10 μm resolution for dynamic acquisitions at 750 Hz top frequency, and 20 mm default measuring range. Two GoPro HERO 5 cameras were also employed to record the subsequent deflected shapes up to buckling (Fig. 4).

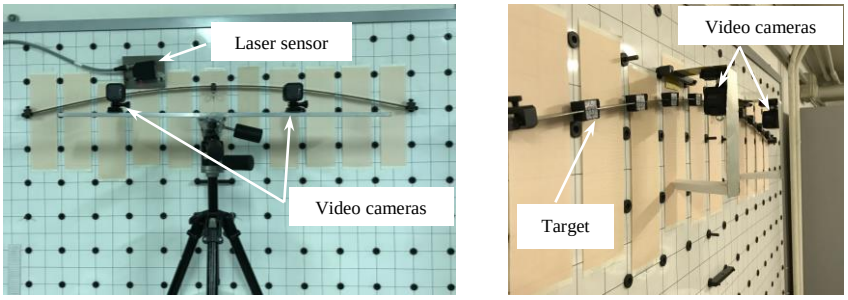

Fig. 4. Experimental set-up for (a) dynamic measurements and (b) static measurements.

4.1 Shape, Geometry and Stiffness Characterization

Given the uncertainties regarding the geometrical and mechanical features, a preliminary characterization was done.

In particular, the arch initial shape was measured both by means of the total station and of some strips of graph paper used as a reference (Fig. 4).

As regards the rectangular thin cross-section, the dimensions were measured by a digital caliper, obtaining the width b = 20 mm and thickness h = 1.5 ± 0.1 mm (un uncertainty of ± 0.1 mm on the thickness was considered, in consideration of its effect on the bending moment of inertia I).

Lastly, direct bending tests were conducted to estimate the bending stiffness EI. The cantilever beam scheme was adopted, considering three free lengths equal to 200, 225, and 250 mm; each cantilever was tested under two different vertical tip forces, respectively equal to 0.87819 N and 1.87852 N. Under each combination of length and force, six reads of the tip deflection were done. The displacements were measured by the same laser sensor already mentioned. The resulting average bending stiffness was $(EI)_{ave}$ = 1,107,946 Nmm^2.

4.2 Static Measurements: Load-Displacement Path

Fig. 5a shows a comparison between experimental and numerical load vs. displacement curves. The experimental curves are limited to the pre-critical phase because the tests were conducted in force-controlled mode. Conversely, the numerical curve also shows the post-peak regime, having been obtained in displacement-controlled mode. As can be seen in Fig. 5a, the two sets of curves show a similar slope (stiffness) of the pre-critical branch. However, the experimental curves exhibited larger values of the peak load compared to the numerical prediction.

Fig. 5b shows a sequence of static configurations, recorded for Test 1. It is clear how the deflection was symmetric at the early load levels, and then switched to the asymmetric configuration as the applied force was increased (compare to Fig. 2).

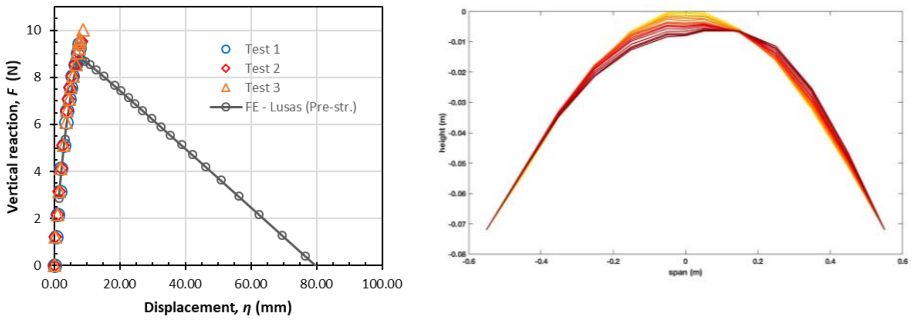

(a) (b)

Fig. 5. (a) Comparison between experimental and numerical load vs. displacement curves and (b) sequence of pre-critical static configurations for Test 1.

4.3 Dynamic Measurements: Fundamental Frequency Variation and Buckling Load Prediction

The decay of the fundamental frequency with the applied force was measured and used to predict the buckling load, according to a classic nondestructive method [5,8]. The dynamic test was repeated three times (Tests 1 to 3). For each loading step, three acquisitions of the free response dynamic signal were done.

Fig. 6a shows the fundamental resonant frequency, f_1, vs. the applied force, F, for the three tests and for the numerical simulation. We see that Tests 1 and 2 showed almost the same trend, while Test 3 exhibited a slightly different behavior, especially in the first phase; this can be ascribed to possible small changes in the initial boundary conditions, to which the system's response is pretty sensitive. Moreover, we observe that the experimental tests exhibited a stiffer response compared to the numerical one, possibly due to some friction in the hinges used in the lab, if not ascribed to an under-estimated stiffness used in the computations. Extrapolating the frequency trend down to zero, provides an estimate of the expected buckling load (this estimate is quite rough).

Plotting the square of the normalized fundamental frequency vs. the applied force reduces the discrepancies between experimental and numerical curves and, also, improves the predictions of the buckling load (linear diagram in theory) [8]; see Fig. 6b ($f_{1,0}$ denotes the fundamental frequency for $F = 0$).

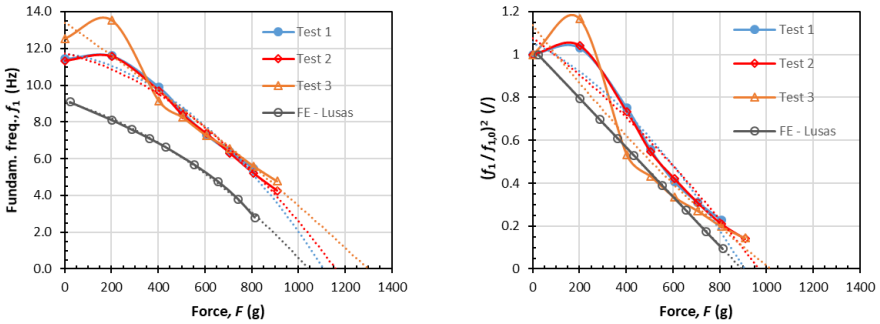

(a) (b)

Fig. 6. (a) Fundamental frequency vs. applied force and (b) normalized fundamental frequency squared vs. applied force: experimental and numerical results.

5 Stability Domains: Form Factors and Imperfection Sensitivity

Stability domains based on form factors are useful tools to separate the effect of different structural parameters on the overall behavior. Given the nonlinearity of the system, this separation does not produce a superimposable set, but if the system is not highly chaotic it produces monotonic trends [9,10]. For flat arches, examples of these factors are the slenderness ratio and the shallowness ratio. Additionally, imperfection patterns or defects can be reduced to geometric factors or metrics. In this study, we made use of two form factors [10], related to the dangerous initial asymmetry of shallow arches. The first one, Δ, is the maximum deviation in absolute value (maximum Euclidean distance) from the ideally perfect axis line (Fig. 7a), whereas the latter, Ω, is the absolute value of the difference between the maximum deviations Δ_l and Δ_r measured on the semi-spans and taken with sign (Fig .7b).

(a) (b)

Fig. 7. Form factors for an imperfect arch: (a) maximum deviation (in absolute value) from the ideal perfect arch, Δ; (b) absolute value of the difference between the maximum deviations measured, with sign, on the semi-spans, Ω.

The reference axis line (perfect) was taken as the sinusoid passing by the hinges and the crown node (with the values of l_0 and f_0 specified in Section 4). Form factors were calculated for every initial shape identified experimentally; an example is shown in

Fig. 8 for Test 1 (compare with Fig. 5b). Interestingly, the maximum values of Δ and Ω correspond to the minimum value of the buckling load (Test 1). Anyway, if Ω acts as an ordering factor for the buckling loads, the intermediate value of Δ was observed for the highest buckling load (Test 3). Table 1 collects the discussed results.

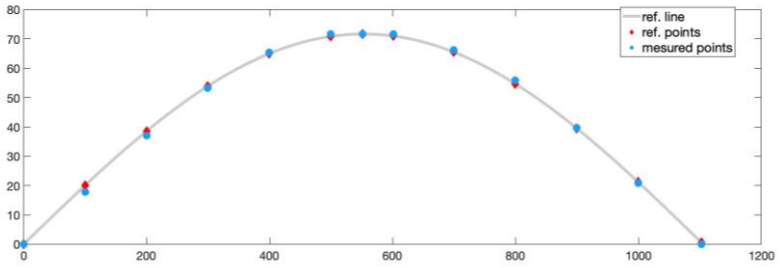

Fig. 8. Initial shape identified for Test 1 (imperfect arch) superposed to the ideal sinusoidal shape (perfect arch).

Table 1. Form factors and critical buckling loads for the three experimental tests.

	Δ (mm)	Ω (mm)	F_c (N)
Test 1	2.172	1.27	9.45
Test 2	1.830	1.12	9.55
Test 3	1.963	0.96	10.0

6 Conclusion

In connection with the problem of bending-active structures, we presented a numerical and experimental investigation on the nonlinear equilibrium paths and the elastic stability of pinned shallow arches obtained by buckling a straight strut and then subjected to a transverse central point load. Finite element analyses were conducted to compare the behavior of the pre-stressed arches with that of the corresponding arches with no initial pre-stress. As an experimental verification, laboratory tests were conducted on a pinned-pinned shallow arch obtained by buckling a thin, slender steel bar. The tested structure was characterized by the following non-dimensional parameters: slenderness ratio of the initially straight bar, $l_n / (I/A)^{0.5}$ = 2,573; rise-to-span ratio, f_0 / l_0 = 0.07; slenderness ratio of the arch (buckled bar), EAl_0^2 / EI = 6.45E+06. The following main conclusions can be drawn.

It was found that the pre-stressing reduces both the stiffness of pre-critical branch and the buckling load of the arch. The instability occurred by nonlinear static bifurcation, with a switch from the symmetric to the asymmetric deformed shape. The dynamic criterion of stability, based on the zero-frequency condition, was effectively used to predict the (static) buckling load. A reasonable agreement was found between experimental and numerical results, although with some differences. Lastly, a suitable

form factor, based only on the identified initial geometry, proved effective in ordering the buckling loads according to the initial geometrical imperfections of the tested arches. Table 2 summarizes the obtained results.

Table 2. Summary of numerical and experimental (only pre-stressed case) results.

Quantity	FE (no pre-stress)	FE (pre-stress)	Test 1	Test 2	Test 3
Nonlin. buckling load, F_c (N)	12.1	8.77	9.45	9.55	10.0
Buckling displ., η_c (mm)	12.5	7.94	7.7	8.2	8.8
Fundam. freq., $f_{1,0}$ (Hz)	12.0	9.10	11.4	11.3	12.5
Predicted buckl. load, F_c^* (N)	12.5	9.10	9.1	9.7	10.2

Further developments of the present work are in due course and will be presented in future contributions.

Acknowledgments

We gratefully acknowledge Prof. Paola Antonaci for allowing us to perform the experimental tests at LaDiSSS lab of Politecnico di Torino – DISEG, as well as Geom. Mauro Perga for making the static measurements by the total station.

References

1. Roorda J (1965) The instability of imperfect elastic structures. Ph.D. Thesis, University College, London.
2. Roorda J (1965) Stability of structures with small imperfections. Journal of the Engineering Mechanics Division 91(1):87–106.
3. Thompson JMT, Hunt GW (1983) On the buckling and imperfection-sensitivity of arches with and without prestress. International Journal of Solids and Structures 19(5):445–459.
4. Virgin NL, Guan Y, Plaut RH (2017) On the geometric conditions for multiple stable equilibria in clamped arches. International Journal of Non-Linear Mechanics 92:8–14.
5. Virgin LN (2007) Vibration of axially loaded structures. Cambridge University Press, New York.
6. Lienhard J, Gengnagel C (2018) Recent developments in bending-active structures. In: Mueller C, Adriaenssens S (eds.) Proceedings of the IASS Annual Symposium 2018 Creativity in Structural Design, pp. 1–8. International Association for Shell and Spatial Structures (IASS).
7. LUSAS Homepage, http://www.lusas.com, last accessed 2023/05/02.
8. Plaut RH, Virgin NL (1990) Use of frequency data to predict buckling load. Journal of Engineering Mechanics 116(10):2330–2335.
9. Auslander J, Yorke JA (1980) Interval maps, factors of maps, and chaos. Tohoku Mathematical Journal, Second Series 32(2):177–188.
10. Bazzucchi F, Manuello A, Carpinteri A (2017) Instability load evaluation of shallow imperfection-sensitive structures by form and interaction parameters. European Journal of Mechanics-A/Solids 66:201–211.